JOURNAL OF MATERIALS SCIENCE 30 (1995) 24–34

# Structural aspects of the ferroelectric phase transition in lanthanum-substituted lead titanate

G. A. ROSSETTI Jr*, L. E. CROSS
*Materials Research Laboratory, The Pennsylvania State University, University Park, Pennsylvania 16802, USA*

J. P. CLINE
*Ceramics Division, The National Institute of Standards and Technology, Gaithersburg, Maryland 20899, USA*

The structural characteristics and ferroelectric phase transition behaviour of chemically derived lanthanum-substituted lead titanate powders have been investigated by high-temperature X-ray diffraction and differential scanning calorimetry. Using X-ray line profile analyses and precise lattice parameter determinations, the important influence of strain coupling through lanthanum/vacancy-induced defect fields on the first-order character of the ferroelectric phase transition was demonstrated. The relaxation of the lattice to the defects as observed in the X-ray measurements was correlated with the onset of diffuse phase transition behaviour revealed by the calorimetry experiments. The lattice relaxation mechanism was connected with the appearance of mesoscopic modulations of the ferroelectric domain structure, and with anomalies in the dielectric behaviour near the transition.

## 1. Introduction

Lead titanate is generally regarded as one of the best-behaved ferroelectric perovskites. Of the seven proper ferroelectric phases allowed by the symmetry of the Pm3m prototype, it exhibits only one confirmed transition at 763 K to a tetragonal P4mm phase [1]. The transition is strongly discontinuous, with a latent heat of at least 1.5 kJ mol$^{-1}$ [2]. Raman spectra show sharp, well-defined modes that all correctly obey the selection rules and disappear abruptly at $T_c$ [3]. Based on inelastic neutron scattering data, $PbTiO_3$ has been seen as a textbook example of a purely displacive ferroelectric [4], although some evidence for a component of order–disorder behaviour has more recently been reported [5]. Nevertheless, the transition behaviour appears to be well described [6–9] by the phenomenological theory of ferroelectricity [10].

At room temperature the tetragonal distortion of lead titanate is large, with lattice constants $a = 0.3899$ nm and $c = 0.4154$ nm [11]. This translates into a spontaneous strain, relative to the prototype at the same temperature, of nearly 5.0% [8]. The tetragonal crystal structure involves only minimal distortion of the oxygen octahedra, and has atomic displacements along the polar axis of $dz_{Ti} = 0.017$ nm and $dz_{O(I)} = dz_{O(II)} = 0.047$ nm relative to Pb at the origin. These displacements give rise to a spontaneous polarization that is unusually large ($\sim 0.75$ C m$^{-2}$) [13, 14].

The break in translational periodicity caused by the introduction of lattice defects leads to rather dramatic changes in the structural properties and ferroelectric phase transition behaviour of lead titanate [15, 16]. An understanding of the role of these defects is important, since doping with aliovalent impurities is commonly used to control the electrical, optical and elastodielectric properties of lead titanate and its technologically important solid solution with lead zirconate.

In this connection, compositions in the system $PbO$–$TiO_2$–$La_2O_3$ (Fig. 1) are of particular interest. The tetragonal distortion ($(c/a) - 1$) of lead titanate is strongly affected by the substitution of lanthanum, and the lattice constants suffer deviations from Vegard's law over a compositional interval extending from approximately 2.5 to 10 at% [18]. This deviation reduces the initial slope of the tetragonal distortion–composition curve by a factor of about four. The behaviour of the cell constants is reminiscent of that observed for lead titanate single crystals subjected to hydrostatic compressive stress [19], where it is found that at room temperature, the transition passes in proximity to a Curie critical point at a critical stress of 1.75 GPa [20]. Indeed, the characteristic first-order discontinuity of the reciprocal permittivity at the

* *Present address*: Department of Geological and Geophysical and Princeton Materials Institute, Princeton University, Princeton, New Jersey 08544, USA.


0022–2461 

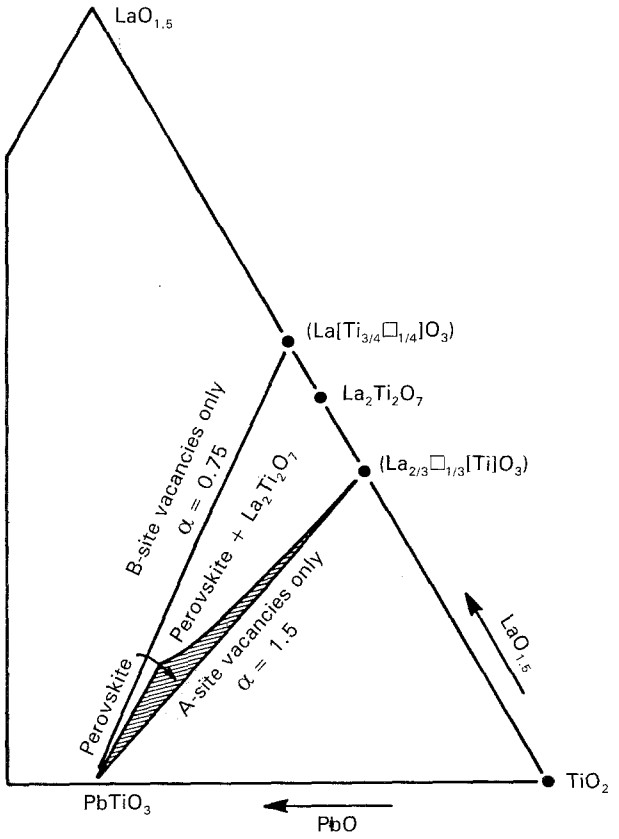


*Figure 1* Partial isothermal section at 1603 K for the $PbO–La_2O_3–TiO_2$ system referring to compositions of general formula $Pb_{1-\alpha y}La_y$ [Ti] $O_3$ (after Hennings [17]).

transition is greatly diminished by the introduction of as little as 0.2 at% lanthanum [21].

In addition to reducing the first-order character of the transition, the substitution of lanthanum induces anomalous or "diffuse" phase transition behaviour characterized by a pronounced smearing of the dielectric susceptibility–temperature curve. Studies of the dielectric properties of ceramic specimens with different grain sizes and lead stoichiometries have demonstrated that a change from conventional to diffuse ferroelectric phase transition behaviour occurs at lanthanum concentrations above about 5 at% [22]. For lanthanum concentrations higher than about 10 at%, the values of the permittivity near the transition are some 100% larger than would be predicted by the generalized Lydanne–Sachs–Teller relationship [23], suggesting that the relaxation of the structural disorder introduced by the lanthanum in some way provides additional contributions to the dielectric response above what is expected from the soft mode theory [24]. This structural disorder appears in the Raman spectra as an additional mode that does not obey the selection rules [25].

The present investigation was undertaken in order to gain a better understanding of the structural factors influencing the breakdown of conventional ferroelectric phase transition behaviour as observed in lanthanum-substituted lead titanate. A series of well-crystallized powder specimens were prepared according to the A-site vacancy formula [17] ($Pb_{1-1.5y}La_y$ [Ti]$O_3$) using a chemical method based on a modification [26] of the solution–gelation (sol–gel) technique developed for lead titanate [27]. The phase transition behaviour of these materials was examined directly by differential scanning calorimetry and by high-temperature X-ray diffraction. The diffractometer employed was specially configured to yield high-quality data on line profile shape. This allowed the temperature evolution of both the macroscopic and microscopic lattice strain to be studied. These data were preferred over data such as might be obtained from ceramic specimens, because they are not likely to be strongly compromised by the effects of elastic boundary conditions, which can be uncertain in densely sintered polycrystalline bodies, and which can influence the phase transition behaviour and ferroelectric properties.

## 2. Experimental procedure

### 2.1. Sol–gel powder synthesis

Powders for calorimetric and X-ray studies were prepared from lead acetate trihydrate, lanthanum isopropoxide and titanium isopropoxide dissolved in 2-methoxyethanol according to a modification of a previously developed procedure [26, 27]. All manipulations of the starting chemicals and reaction mixtures were carried out under anhydrous conditions in a Braun glove box fitted with a recirculating dry nitrogen purge and liquid nitrogen cooled vapour trapping system. The box atmosphere was sufficiently dry ( $\leqslant 5$ p.p.m. $H_2O$) that no fuming was visually detectable on exposure to diethyl zinc.

In each case, the preparation was based on 16.8 mmol of titanium isopropoxide, which was measured out volumetrically using a microlitre pipet. The corresponding amounts of lead acetate trihydrate and lanthanum isopropoxide required to make samples with $y = 0$, 0.005, 0.01, 0.02, 0.035, 0.05 and 0.15 according to the formula $Pb_{1-1.5y}La_y$ [Ti]$O_3$ were weighed out on an electronic balance precise to 1 mg. The required distillation and refluxing operations of the starting solutions were conducted under dry argon purge in a standard glass distillation apparatus utilizing ground-glass joints. The refluxing was continued until the temperature of the vapours condensing in the still head reached that of the boiling point of the pure solvent.

The water for hydrolysis (4 mol per mol alkoxide) was introduced to the reaction mixture at $< 250$ K as a solution in 2-methoxyethanol. Transparent amber-coloured gels were obtained on warming this mixture to room temperature. After volatilizing the entrapped solvent, the gel products were gently powdered in a mortar and were calcined on platinum foil within a closed, virgin, alumina crucible. The maximum calcining temperature was 1323 K (1 h) with intermediate holds on heating at 623 K (1 h) and 1073 K (3 h). The resultant light yellow powders were examined by transmission electron microscopy and showed no evidence of second phases, amorphous material, or incomplete or inhomogeneous reaction. The nominal compositions of the powders were checked by comparing the tetragonal distortion determined by X-ray diffraction against the previously reported values [18].

## 2.2. X-ray measurements

X-ray powder diffraction data were collected on a Siemens D500 diffractometer equipped with an incident-beam monochromator and scanning linear position-sensitive detector (PSD). The monochromator consisted of a focusing crystal of germanium that virtually eliminated the peaks associated with the $K_{\alpha 2}$ component of the Cu radiation. The near elimination of the bremsstrahlung resulted in reduced intensity in the tail region of the diffraction peaks and increased the peak to background ratio. The use of the PSD resulted in dramatic increases in the diffraction signal. Although this gave rise to some small increase in the peak width, as an overall indication of the resolution of the system, the typical full width at half maximum for the Bragg peaks of a lanthanum hexaboride reference standard (Standard Reference Material No. 660) was approximately 0.06° in 2θ. Ambient temperature data were collected using zero-background quartz plates on to which the specimens were uniformly deposited from an isopropanol suspension. The scan ranges were from 18 to 98° 2θ with a step increment of 0.01° and a scan rate for the PSD of 0.6° $min^{-1}$. With a PSD window of 4.67°, this translated into a count time of 7.78 min per step.

High-temperature data were collected on the same diffractometer fitted with a Bühler hot stage utilizing two platinum heaters. The first of these was a strip heater on which the specimen resided during analysis. A second heater surrounded the first and was positioned to reduce temperature gradients. The temperature was measured with a type S thermocouple welded to the underside of the heating strip. The scan range and step increment were the same as those used in the collection of the room-temperature data, but the scan rate was increased to 1.25° $min^{-1}$ (count time = 3.86 min per step). The data were collected in 5 K increments straddling the anticipated cubic → tetragonal transition temperature by 20 K, and in 10 K increments straddling this temperature by 40 K. All data were collected on cooling, with additional data collected at 100 K increments as the specimen cooled to the final temperature of 373 K. The data were collected in an air atmosphere.

All data analysis was performed using the Siemens DIFFRAC 5000 software. Lattice parameters were determined by the least-squares refinement method using 15–20 of the tetragonal reflections and all of the cubic reflections appearing in the scan range. The peak positions were determined using a variable tip-width peak-locating algorithm based on a second-derivative test. The results of the algorithm were visually inspected by expanding each peak region on a monitor, and manual corrections to the peak positions were made when necessary.

The peak positions so determined were corrected by applying a calibration curve generated by fitting a second-order polynomial to the known peak positions for the lanthanum hexaboride (SRM 660) external reference standard. Using this procedure, the absolute angular precisions of the least-squares fits for pure lead titanate at room temperature seldom exceeded 0.005° 2θ. For reasons that will become evident, the precision of the fits for the lanthanum-modified specimens varied somewhat, but were almost always better than 0.025° 2θ. A comparable precision was achieved in the fits of high-temperature data. Because of the smaller tetragonal distortion and more pronounced broadening of the diffraction profiles observed for the specimen with $y = 0.05$, this procedure proved impractical in analysing the high-temperature data. Instead, the peak positions of the 213/312/321 reflections for this specimen were determined by deconvolution and these were then used to calculate the lattice parameters. More scatter in the data for this sample was therefore observed.

Line profile analyses were conducted by fitting the diffraction profiles to split Pearson distributions. Pearson type VII distributions are of the form [28]

$$y(x) = y_0\left(1 + \frac{(x - \bar{x})^2}{ma^2}\right)^{-m} \quad (1)$$

with $y_0 = y(\bar{x})$. The full width β at the $(1/p)$th maximum is

$$\beta\left(\frac{y_0}{p}\right) = 2a[m(p^{1/m} - 1)]^{1/2} \quad (2)$$

The function varies from Lorentzian when $m = 1$ to Gaussian in the limit $m = \infty$. The split distributions allowed the profile shape on the low and high angle sides of $\bar{x}$ to be fitted with separate exponents, $m^L$ and $m^H$. These distributions gave two values for the corresponding equivalent full width at half maximum (FWHM), $\beta^L$ and $\beta^H$, and so permitted the investigation and quantification of the profile symmetry.

## 2.3. Calorimetry

Differential scanning calorimetry (DSC) was performed using two calorimeters. Estimates of the phase transition temperatures were made using a Perkin Elmer DSC-2C calorimeter calibrated to a zinc foil reference standard. The samples (40 to 60 mg in size) were weighed out on an electronic microbalance that was precise to 0.01 mg and were sealed in aluminium capsules. The measurements were made in heating runs performed under a dry nitrogen purge using a scan rate of 2.5 K $min^{-1}$. Transition temperatures were estimated directly from the calorimeter power versus temperature curves using the Perkin Elmer software. Prior to the experiments, the operational controls of the instrument were carefully adjusted to achieve a degree of baseline flatness sufficient for these estimations to be readily made without applying baseline slope or curvature corrections. Although enthalpies of transition could also be estimated from these data, the signal from the higher lanthanum content materials was weak, and not suitable for analysis.

Consequently, the enthalpies of transition of selected samples were measured using a Setaram TG-DSC 111 calorimeter operated in the horizontal configuration. The Setaram DSC is a microcalorimeter of the twin Calvet design. The temperature of the instrument was calibrated to the melting points of high-purity (99.999 + %) In, Pb, Zn and Al. Power calibration was performed electrically using a Joule effect

device. Again, the samples were weighed out on an electronic balance that was precise to 0.01 mg and were sealed in aluminium crucibles. The measurements were made in heating runs in a static air atmosphere at scan rates of 1–5 K $min^{-1}$.

For the purposes of comparing the transition behaviour of the various specimens, enthalpies of transition were estimated directly from the power versus temperature curves using a thermal analysis software package (Astra Scientific International). The procedure adopted for carrying out the integration of these curves was tested by measuring the enthalpy of the $\alpha \rightarrow \beta$ transition for a high-purity synthetic quartz sample. The transition enthalpy so obtained was 0.610 kJ $mol^{-1}$ and was reproducible to within $\sim$ 0.03 kJ $mol^{-1}$. This result was in good agreement with the recent literature value of 0.625 kJ $mol^{-1}$ [29]. However, it must be emphasized that, although useful for comparative purposes, the transition enthalpies obtained in this way should be regarded as estimates. A more detailed analysis of precise heat capacity data would be required to accurately determine these values.

## 3. Results and analysis

### 3.1. Structural studies

An X-ray powder diffraction pattern collected on the sol–gel derived lead titanate at room temperature is shown in Fig. 2. The high degree of crystallinity evident in the pattern is representative of that observed for all of the specimens examined. The peak intensity on the 100% peak varied from 1500 to 3000 c.p.s. depending on the lanthanum concentration, while the background signal seldom exceeded 20 c.p.s. Consequently, no background subtraction, smoothing or other data corrections were required. Careful inspection and fitting of the background around a variety of $h\,k\,l$ reflections across the entire scan range revealed no reflections associated with secondary phases, and no anomalous background scattering could be detected.

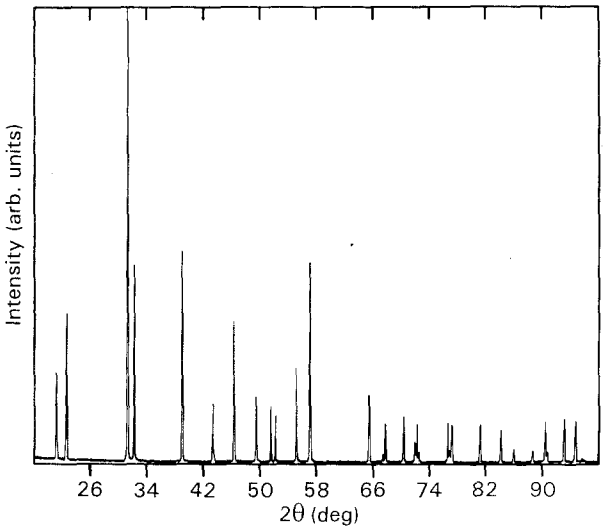


*Figure 2* X-ray powder diffraction pattern for lead titanate at room temperature ($CuK_{\alpha 1}$ radiation).

In order to gain some insight into the effect of lanthanum substitution on the intrinsic shapes and breadths ($\beta$) of the diffraction profiles, a split Pearson analysis of the 3 0 0 reflection was conducted at a temperature above the expected Curie point at $T \sim T_c + 35$ K. The results of the analysis are shown in Table I. The shapes of the diffraction profiles for all specimens were found to be nearly symmetric and were predominantly Lorentzian in shape. For the samples with lanthanum concentrations $y < 0.020$, no significant broadening of the diffraction profiles relative to the profile for unmodified lead titanate was observed, and the full width at half maximum was approximately 1.5–2 times that of the expected resolution of the instrument. For $y > 0.020$, some additional broadening of the diffraction profiles became apparent.

The room-temperature FWHM values for selected reflections of samples with different lanthanum concentrations are collected in Table II. Several important trends in these values were observed. First, for all reflections and compositions investigated, a significant increase in line breadth over that observed for unmodified lead titanate was evident. For each reflection, the composition dependence of the FWHM value was qualitatively similar, with the magnitude of the broadening increasing between $y = 0$ and $y = 0.05$ but then decreasing when the lanthanum concentration was further increased to $y = 0.15$. The broadening of the diffraction profiles was most pronounced in the peaks that had high $l$-component indices, such as the 0 0 2, 0 1 2 or 2 2 2 reflections. For all of the lanthanum-substituted materials, the ratio $\beta_{0\,0\,l}/\beta_{h\,0\,0} \sim 2.0$ was significantly greater than the corresponding value ( $\sim$ 1.2) observed for lead titanate. Although this result implies that the incorporation of lanthanum induces a structural distortion associated primarily with a variance in the $c$ lattice parameter, the significant broadening of the $h\,0\,0$ reflections suggests that some variance in the $a$ lattice parameter also occurred.

Marked changes in the shape of the diffraction profiles relative to unmodified lead titanate were also observed. Table III shows that the diffraction profiles for the lanthanum-modified materials exhibited a significantly greater degree of asymmetry than those for the pure compound. As with the FWHM value, the degree of the asymmetry was most obvious in the peaks having high $l$-component indices. This can be visually ascertained from Fig. 3, where the shapes of the 0 0 2 and 2 0 0 profiles for lead titanate and a lanthanum-modified sample are compared. In this figure the crosses represent the raw data points, and the solid lines represent the best approximation of the profile shape obtained by the split Pearson fitting. The fitted curves are plotted less background in order that the shapes of the profiles may be more easily appreciated. The horizontal line in the centre of each figure represents the difference curve between the measured data points and the fitted values. The quality of the fits as determined by the reliability index

$$R = \left( \frac{\Sigma[I(\text{obs}) - I(\text{calc})]^2}{\Sigma[I(\text{obs})]^2} \right)^{1/2} \quad (3)$$

TABLE I Split Pearson analysis of the 300 reflection of $Pb_{1-1.5y}La_y$ [Ti]$O_3$ at $T \simeq T_c + 35$ K

| La content, $y$ | $\beta^L$ (deg 2θ) | $\beta^H$ (deg 2θ) | $\beta$ (deg 2θ) | $m^L$ | $m^H$ |
|---|---|---|---|---|---|
| 0 | 0.081(2) | 0.096(2) | 0.089(2) | 0.75(3) | 0.90(4) |
| 0.005 | 0.112(2) | 0.103(2) | 0.108(2) | 1.7(1) | 1.3(0.9) |
| 0.010 | 0.098(2) | 0.091(2) | 0.095(2) | 1.1(0.6) | 1.0(0.5) |
| 0.020 | 0.132(4) | 0.121(4) | 0.127(4) | 1.1(0.7) | 1.1(0.9) |
| 0.035 | 0.155(5) | 0.133(5) | 0.144(5) | 0.90(6) | 0.89(7) |
| 0.050 | 0.208(9) | 0.208(9) | 0.208(9) | 0.73(6) | 0.92(9) |

The numbers in parentheses represent the standard deviation in the least significant digit.

TABLE II FWHM for various reflections of $Pb_{1-1.5y}La_y$ [Ti]$O_3$ at room temperature

| Reflection *hkl* | FWHM(deg. 2θ) | | | | | | |
|---|---|---|---|---|---|---|---|
| | $y = 0$ | $y = 0.005$ | $y = 0.010$ | $y = 0.020$ | $y = 0.035$ | $y = 0.050$ | $y = 0.150$ |
| 001 | 0.116(2) | 0.178(2) | 0.278(6) | 0.280(6) | 0.272(6) | 0.299(7) | 0.219(8) |
| 100 | 0.099(0.9) | 0.131(0.9) | 0.164(1) | 0.163(1) | 0.162(1) | 0.174(2) | 0.150(2) |
| 101 | 0.092(0.3) | 0.130(0.5) | 0.190(1) | 0.202(1) | 0.195(1) | 0.214(1) | 0.163(0.8) |
| 110 | 0.091(0.9) | 0.129(1) | 0.174(3) | 0.179(2) | 0.178(2) | 0.196(3) | 0.175(2) |
| 111 | 0.085(0.4) | 0.116(1) | 0.163(1) | 0.183(1) | 0.173(1) | 0.191(1) | 0.150(1) |
| 002 | 0.105(1) | 0.252(7) | 0.486(13) | 0.492(17) | 0.478(14) | 0.494(17) | 0.342(12) |
| 200 | 0.086(0.4) | 0.134(1) | 0.205(2) | 0.213(2) | 0.209(2) | 0.229(2) | 0.168(2) |
| 012 | 0.099(1) | 0.226(4) | 0.425(10) | 0.465(11) | 0.415(11) | 0.455(13) | 0.341(18) |
| 201 | 0.084(1) | 0.134(3) | 0.200(6) | 0.223(6) | 0.224(7) | 0.254(11) | 0.196(13) |
| 210 | 0.085(1) | 0.143(3) | 0.217(7) | 0.227(7) | 0.235(8) | 0.267(14) | 0.192(15) |
| 222 | 0.103(2) | 0.192(4) | 0.324(10) | 0.378(12) | 0.368(13) | 0.406(12) | 0.320(10) |

The numbers in parentheses represent the standard deviation in the least significant digit.

TABLE III Split Pearson analysis for various reflections of $Pb_{1-1.5y}La_y$[Ti]$O_3$ at room temperature

| Reflection *hkl* | $y = 0$ | | $y = 0.01$ | |
|---|---|---|---|---|
| | $\beta^L$ | $\beta^H$ | $\beta^L$ | $\beta^H$ |
| 001 | 0.145 | 0.087 | 0.209 | 0.347 |
| 100 | 0.120 | 0.078 | 0.197 | 0.129 |
| 101 | 0.109 | 0.075 | 0.154 | 0.225 |
| 110 | 0.107 | 0.074 | 0.214 | 0.132 |
| 111 | 0.094 | 0.076 | 0.155 | 0.171 |
| 002 | 0.107 | 0.102 | 0.223 | 0.748 |
| 200 | 0.099 | 0.071 | 0.261 | 0.149 |
| 012 | 0.099 | 0.100 | 0.237 | 0.612 |
| 201 | 0.084 | 0.085 | 0.202 | 0.196 |
| 210 | 0.094 | 0.076 | 0.285 | 0.149 |
| 222 | 0.093 | 0.113 | 0.267 | 0.379 |

The standard deviations in the least significant digit are similar to those reported in Table II.

depended to some extent on the lanthanum concentration, but the $R$ value typically increased from as low as $R \simeq 0.015$ for the 001 reflection to $R \simeq 0.065$ for the 222 peak.

As an overall indication of the profile asymmetry, the composition dependencies of the ratio $\beta^H/\beta^L$ for the 002 and 200 reflections are compared in Fig. 4. As seen in the figure, the behaviour of $\beta^H/\beta^L$ for the 002 reflection is the mirror image of that for the 200 peak, with both ratios having sharp extrema centred near the composition $y = 0.01$. The strong coupled asymmetry for these reflections combined with the increase in overall peak breadth suggests that a distortion associated with a non-uniform variance in the crystal tetragonality ($c/a$) existed in all of the lanthanum-modified compositions investigated. The degree of the non-uniformity decreased sharply between $y = 0.01$ and $y = 0.05$ but did not change significantly on further increasing the lanthanum content to $y = 0.15$.

Lattice parameters for the samples investigated are listed in Table IV. As expected from previously reported data, the lattice distortion along the tetragonal $c$ axis was much more strongly affected by the incorporation of lanthanum than was the distortion along the $a$ axis. The crystal tetragonality $c/a = 1.0649$ determined for unmodified lead titanate powder compares favourably with the single-crystal value 1.0653 determined using the Debeye–Scherrer camera method [11]. It is interesting to note that the standard errors of the refinements appeared to pass through a maximum centred near the composition $y = 0.02$. This was most likely a result of the marked peak asymmetry near this composition, which made the assignment of the peak positions somewhat more uncertain. Nevertheless, the standard errors for all specimens were of similar magnitude and were quite small ($10^{-5}$ nm).

The values of $a$ and $c$ listed in Table IV are plotted in Fig. 5. As previously observed for mixed oxide specimens [18], pronounced deviations from Vegard's law are apparent for both the $a$ and $c$ lattice parameters. Based on the changes in diffraction profile symmetry (Fig. 4), and on the fact that all of the specimens were prepared according to the A-site va-

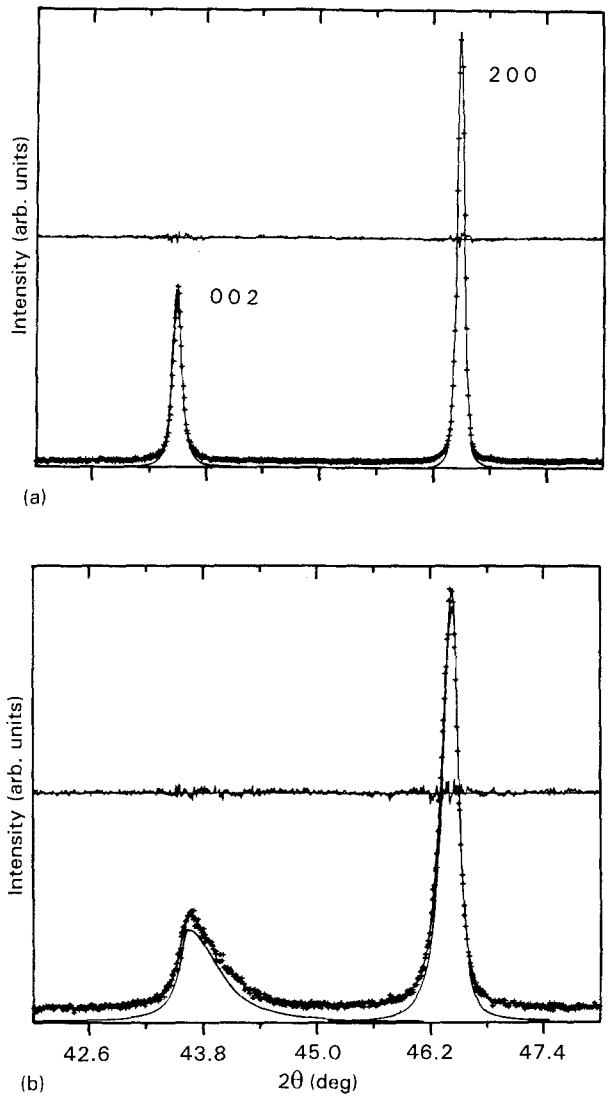


*Figure 3* Split Pearson fitting of the 002/200 reflections of $Pb_{1-1.5y}La_y$ [Ti]$O_3$ for (a) $y = 0$ and (b) $y = 0.01$. (Cu $K_{\alpha_1}$ radiation).

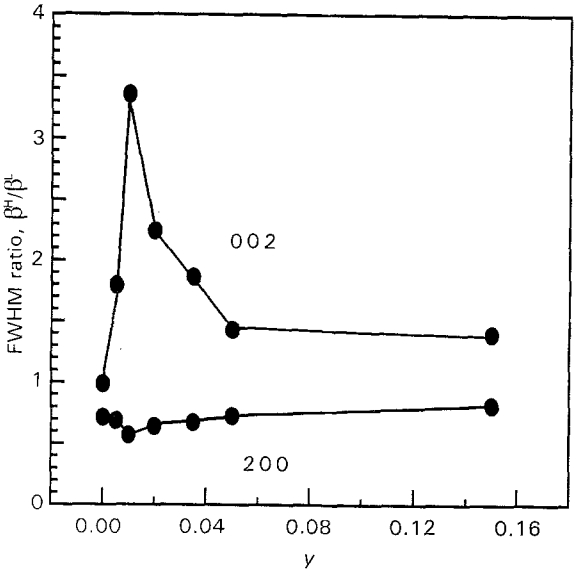


*Figure 4* Peak asymmetry of the 002/200 reflections of $Pb_{1-1.5y}La_y$ [Ti]$O_3$.

TABLE IV Lattice parameters of $Pb_{1-1.5y}La_y[Ti]O_3$ at room temperature

| La content, $y$ | $a$ (nm) | $c$ (nm) | $c/a$ |
|---|---|---|---|
| 0 | 0.38997(0.5) | 0.41529(1) | 1.0649 |
| 0.005 | 0.39014(0.8) | 0.41444(2) | 1.0623 |
| 0.010 | 0.39032(2) | 0.41367(5) | 1.0598 |
| 0.020 | 0.39055(3) | 0.41156(6) | 1.0538 |
| 0.035 | 0.39082(2) | 0.40961(4) | 1.0481 |
| 0.050 | 0.39098(2) | 0.40734(4) | 1.0418 |
| 0.150 | 0.39166(2) | 0.39867(3) | 1.0179 |

The numbers in parentheses represent the standard errors obtained from least-squares refinement.

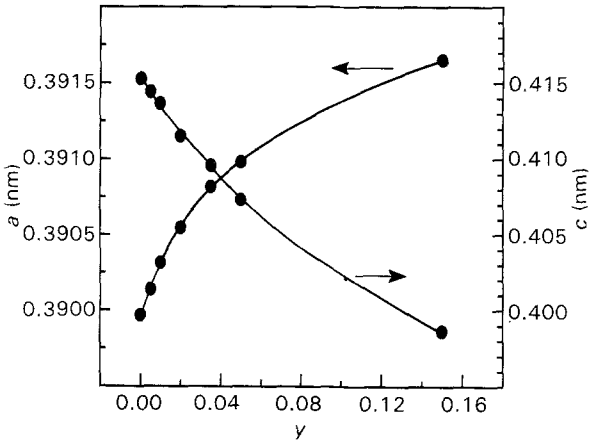


*Figure 5* Lattice parameters of $Pb_{1-1.5y}La_y$ [Ti]$O_3$ at room temperature.

cancy formula, it is proposed that this deviation results from a lattice relaxation mechanism as opposed to a change in the vacancy site distribution as suggested earlier [18].

To better understand the nature of this relaxation mechanism, the temperature dependence of both spontaneous and lattice strains was examined. The spontaneous strain is related to the tetragonal distortion ($(c/a) - 1$) and so may be determined from the lattice constants. The results for specimens with $y = 0.0$–$0.05$ are shown in Fig. 6. The relative degree of lattice strain as a function of composition and temperature was qualitatively assessed from a measurement of the FWHM of the 2 2 2 reflection. The 2 2 2 reflection is not split by the tetragonal symmetry, and so the temperature dependence of the FWHM can be conveniently compared both above and below the transition temperature. Based on the data in Table II, this reflection also showed a marked broadening related to the lanthanum concentration.

Representative results for a specimen of composition $y = 0.01$ are shown in Fig. 7a. On cooling through the transition a large change in lattice strain occurred, as indicated by the abrupt discontinuity in the FWHM value near $T_c$. Despite this, as shown in Fig. 7b, no unusual or anomalous behaviour could be detected in the temperature dependence of the lattice constants near the transition. It should be recalled, however, that in the vicinity of a first-order transition,

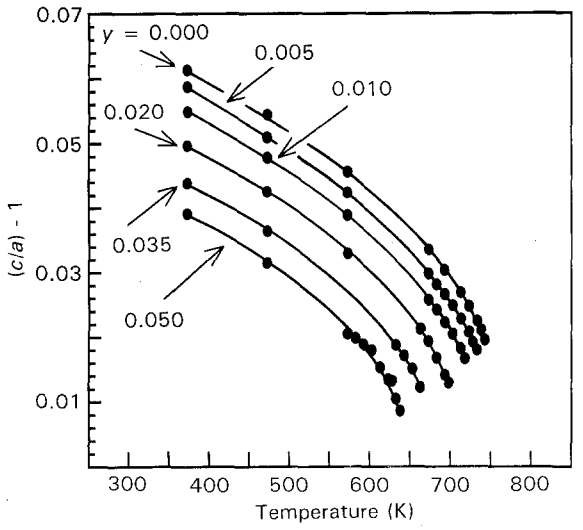


*Figure 6* Temperature dependence of the tetragonal distortion $(c/a) - 1$ for $Pb_{1-1.5y}La_y$ [Ti]$O_3$.

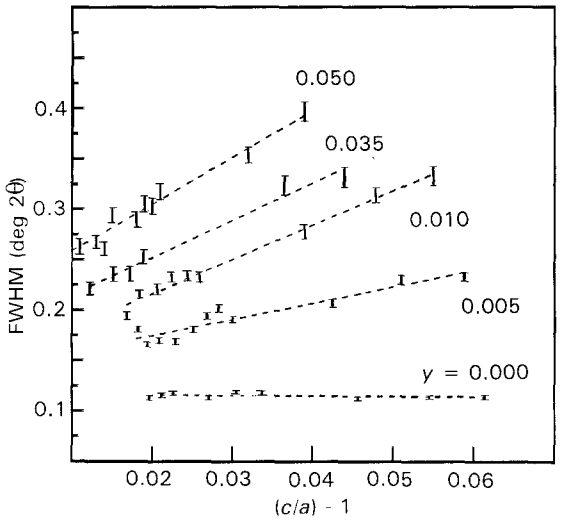


*Figure 8* Influence of tetragonal distortion $(c/a) - 1$ on the FWHM of the 2 2 2 reflection for $Pb_{1-1.5y}La_y$ [Ti]$O_3$.

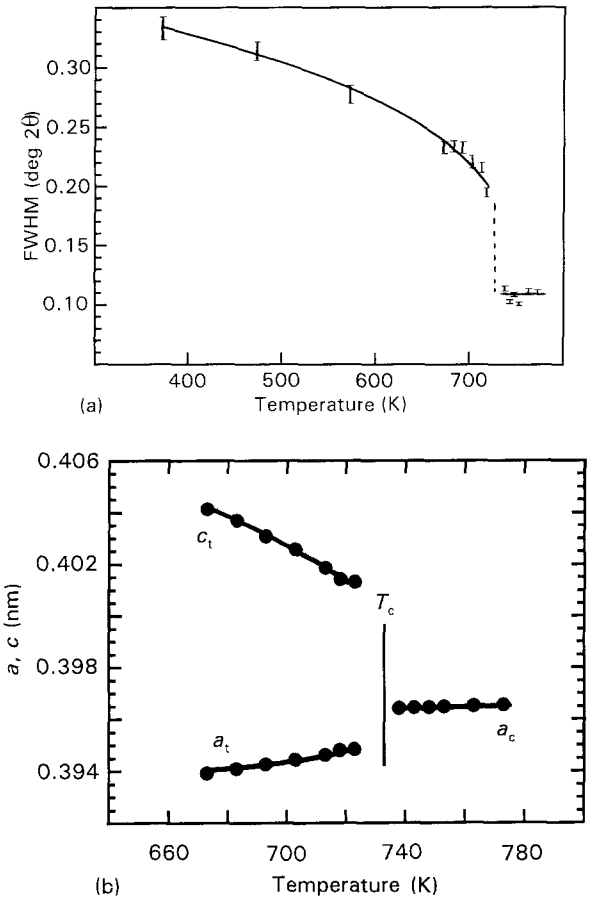


*Figure 7* Temperature dependence of the FWHM of the 2 2 2 reflection of $Pb_{1-1.5y}La_y$ [Ti]$O_3$ ($y = 0.01$) (a). The associated variation in the lattice parameters (b).

some discontinuity in peak breadth is expected due to the overlap of tetragonal and cubic reflections occurring in the coexistence region of the two phases. The data for such profiles are not shown in the figure and were readily identified because considerably poorer fitting, as indicated by a sharp increase in the reliability index, was observed when peaks from both phases were present.

The temperature dependence of the line breadth data in Fig. 7 suggested that the increased FWHM values relative to the pure specimen as observed at room temperature were directly related to the degree of tetragonal distortion. As shown in Fig. 8, the tetragonal distortion ($(c/a) - 1$) when plotted against the FWHM for the 2 2 2 reflection did in fact yield a family of approximately straight lines with slopes and intercepts dependent on the lanthanum concentration. The large change in slope occurring between $y = 0$ and $y = 0.01$ is indicative of the strong initial relaxation of the lattice due to the effects of the dopant. The observed $c/a$ dependence of the peak breadth combined with the marked profile asymmetry in the 0 0 2/2 0 0 reflections suggests that the primary contribution to the broadening as observed in the diffraction data at room temperature results from the relaxation of the uniform tetragonal distortion due to the incorporation of the lanthanum.

In fact, recent *in situ* transmission electron microscopy studies [30] of lanthanum-substituted lead titanate ceramics have revealed the presence of sub-domain modulations oriented primarily along the tetragonal $c$ axis, which is mechanically the softest [19]. The modulated textures occurred on a scale of $\sim 10$ nm within well-defined ferroelectric domains, in which there must exist an average, but spatially varying, polarization $\bar{P}$. Such microstructures are not unique to ferroelectrics, and are commonly observed in ferroelastic minerals and materials formed via kinetic processes, that is, under conditions where cation-ordering reactions have occurred incompletely or inhomogeneously or in crystals that are otherwise not at equilibrium [31]. As seen in Fig. 9, these modulations first became obvious at a lanthanum concentration of $y \simeq 0.05$ and developed into a cross-hatched or "tweed" texture on reaching $y \simeq 0.25$. These textures were found to disappear on heating above the transition temperature, and so could not be associated with exsolution lamellae. As can be appreciated from the data in Table II and Fig. 4, the appearance and extent of the sub-domain texture correlates well with the

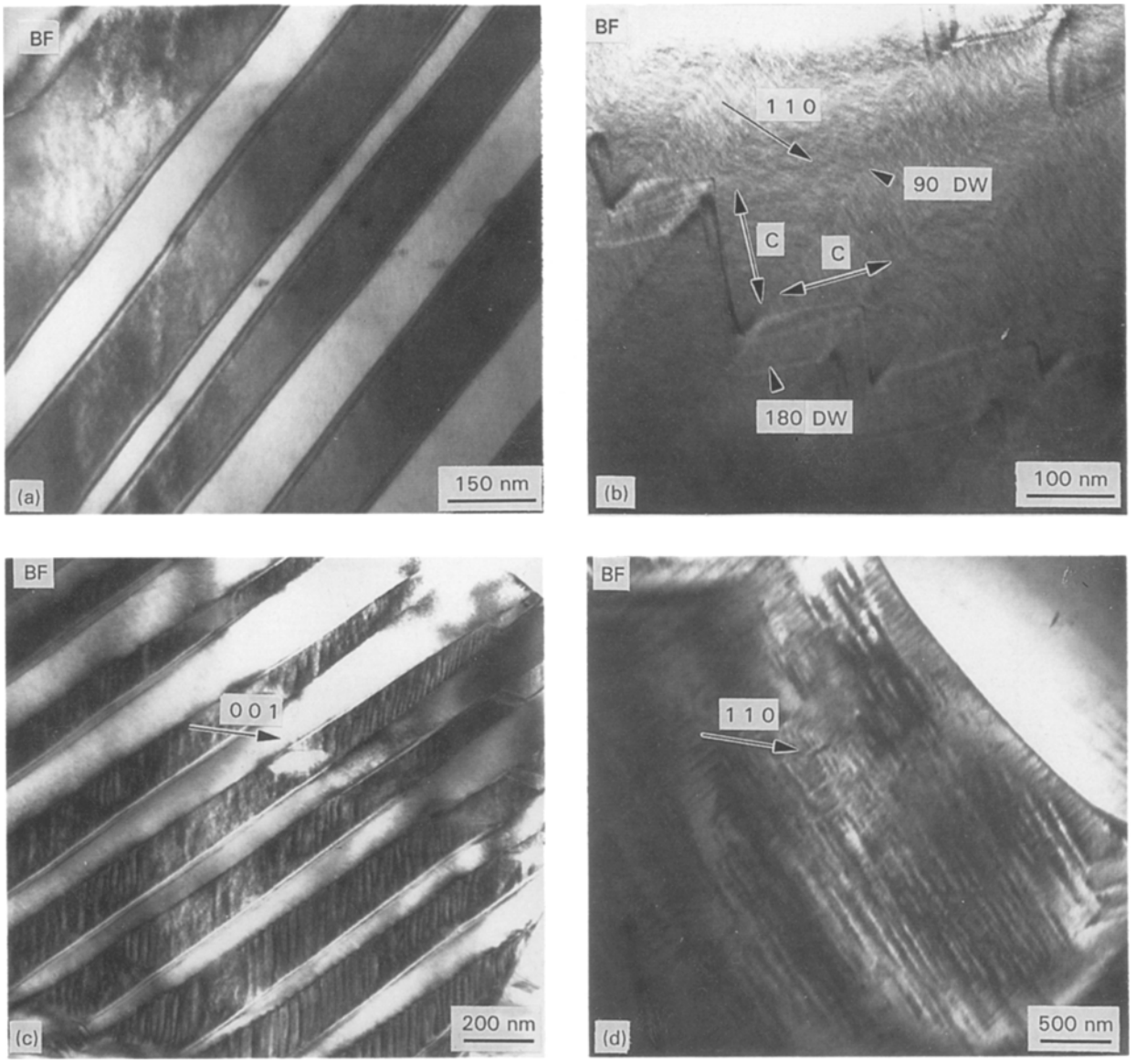


*Figure 9* Transmission electron micrographs showing the modulated ferroelectric domain structure as observed for $Pb_{1-1.5y}La_y$ [Ti]$O_3$: (a) $y = 0.01$, (b) $y = 0.05$, (c) $y = 0.10$, (d) $y = 0.25$ (after Randall *et al.* [30]).

changes in profile breadth and symmetry found in the diffraction experiments.

It should be noted that the data presented here are consistent neither with particle size effects nor with the existence of macroscopic inhomogeneities in the chemical composition. Observations arguing against the influence of these two effects are (i) the temperature dependence of the profile broadening below the Curie point; (ii) the inherent homogeneity achievable with the sol–gel process; (iii) the pronounced asymmetry of the diffraction profiles for all of the $hkl$ reflections investigated (composition fluctuations should give a random distribution in $c/a$); and (iv) that the profile breadth decreased when the dopant level was increased above $\sim 5$ at%.

## 3.2. Phase transition behaviour

In investigating the influence of these structural changes on the phase transition behaviour, it proved informative to analyse the scalar strain data (Fig. 6) as though all of the specimens were close to a Curie critical transition. At a Curie critical instability, the order of the transition changes, and the temperature dependence of the order parameter (i.e. the spontaneous polarization) is given by

$$P(T) \propto [(c/a) - 1]^{1/2} \propto (T_c - T)^{1/4} \qquad (4)$$

Consequently, plots of $[(c/a) - 1]^2$ versus $T$ should give a good indication of any changes in the nature of the phase transition as the lanthanum content is increased. The results of this analysis are shown in Fig. 10a, where it is seen that Equation 4 holds approximately for all of the specimens investigated. However, as shown in Fig 10b, the absolute values of the slopes of the lines so obtained decreased with increasing dopant concentration, with the rate of decrease in slope with composition changing to a smaller value for samples with $y \geqslant 0.02$. This decrease in slope reflects the more continuous nature of the transition.

Additional insight into the meaning of this observation was gained from the calorimetry data. Normalized

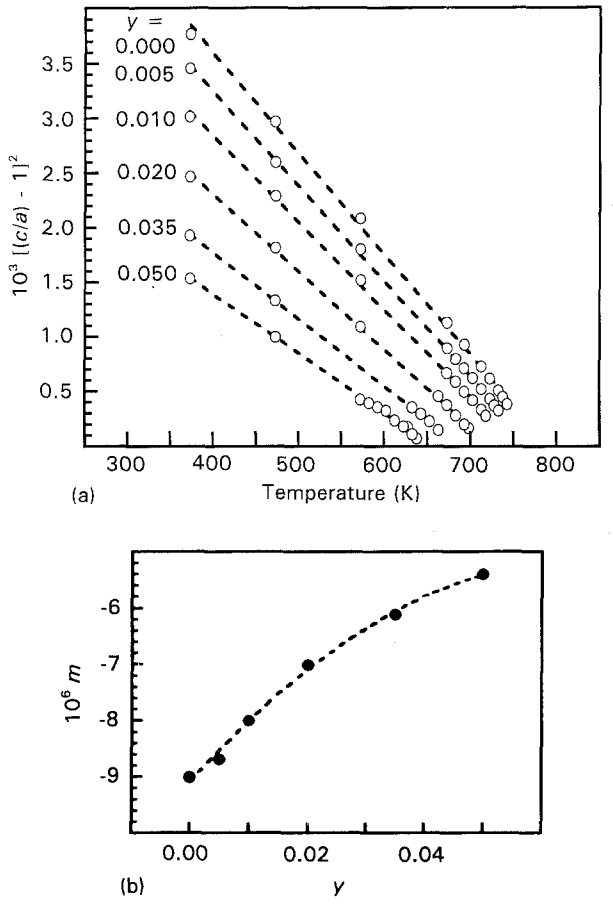


*Figure 10* Plots of $[(c/a)-1]^2$ versus $T$ for $Pb_{1-1.5y-}La_y\,[Ti]O_3$ (a). The composition dependence of the slope $m$ of the curves (b).

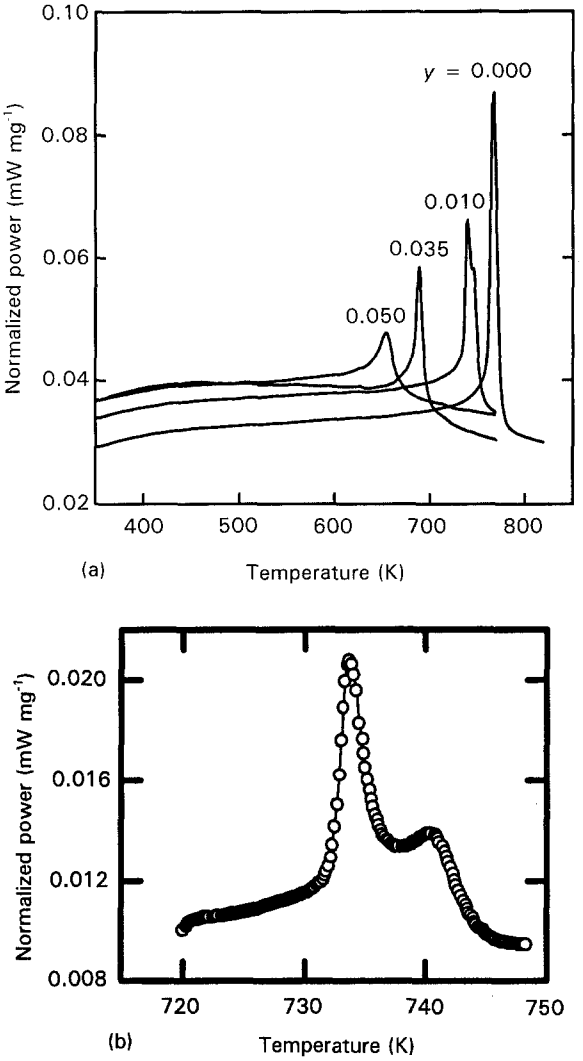


*Figure 11* DSC curves for $Pb_{1-1.5y}La_y\,[Ti]O_3$ obtained in heating runs at 5 K min$^{-1}$ (a). The anomalous behaviour observed for the specimen with $y = 0.01$ as obtained at a slower heating rate of 1 K min$^{-1}$ (b).

power versus temperature curves for the various specimens investigated are shown in Fig. 11a. The transition enthalpies obtained by the direct integration of these curves are shown in Fig. 12. It was found that the transition enthalpy dropped substantially between $y = 0.00$ and $y = 0.01$, but after the initial drop did not change significantly with subsequent increases in lanthanum concentration. Despite the rather dramatic changes in the nature of the phase transition, the shift in transition temperature with composition was nearly linear, with a slope $dT_c/dy = -20.9$ K per at% La. This value is in good agreement with the value of $-19.9$ K per at% obtained from dielectric measurements made on dense ceramic specimens over a much wider range of composition extending from $y = 0.04$ to $y = 0.30$ [22].

Corresponding to the initial drop in the transition enthalpy, a small anomaly in the DSC curves was detected. As shown in Fig. 11b, even at scan rates as low as 1 K min$^{-1}$ this anomaly was not resolved into separate enthalpic events. The anomaly was observed both on heating and cooling, and showed a reproducible thermal hysteresis that occurred after repeated cycling through the transition. This behaviour was detected in both the Perkin Elmer and Setaram calorimeters, and so was not an artefact of the measurement technique. Furthermore, it was evident only in the samples with $y = 0.005$ and 0.01, and could not be detected for unmodified lead titanate or for samples

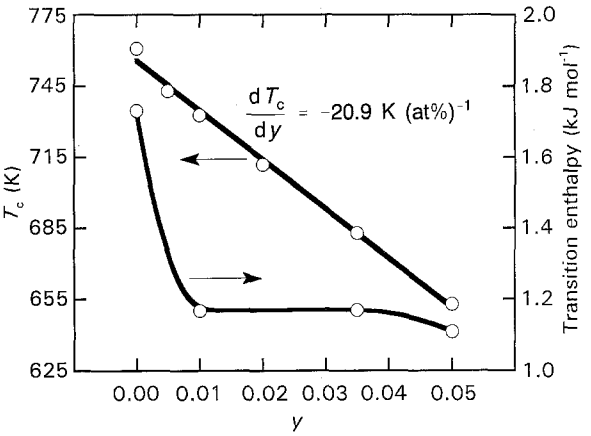


*Figure 12* Estimated transition temperatures and enthalpies of $Pb_{1-1.5y}La_y\,[Ti]O_3$.

with lanthanum contents higher than $y = 0.01$. Based on the diffraction profile data presented in Figs 4 and 8, it is proposed that this anomalous behaviour reflects the breakdown of conventional first-order ferroelectric

phase transition behaviour as the lattice relaxes to the defects and long-range order is disrupted.

Specimens with higher lanthanum concentrations did not exhibit the anomalous transition behaviour, but instead exhibited broadened DSC peaks indicative of a smeared phase transition. Consequently, for specimens with $0.02 \leqslant y \leqslant 0.05$, the apparent changes in the nature of the transition as revealed in the diffraction data of Fig. 10 can be associated with the change-over from conventional to diffuse transition behaviour. For the specimen with $y = 0.05$, the transition was very diffuse and took place over a temperature interval that was estimated to be as much as 150 K. Indeed, as shown in Fig. 13, local distortions of the structure connected with the smearing of the transition could be detected as a temperature-dependent X-ray profile broadening that continued above the expected transition temperature. Fig. 14 shows that as a result of this smearing, the signature of the first-order discontinuity of the transition was obscured, and the transition appeared to take place in a continuous manner. Similar behaviour has also been observed in synchrotron studies of lightly doped barium titanate [32].

## 4. Discussion

For specimens prepared according to the A-site vacancy formula, the introduction of lanthanum to lead titanate produces one lead vacancy for every two La (III) ions. These defects locally break the translational periodicity of the lattice and produce elastic and electric fields that fall off slowly as a function of distance from the defect cores [33]. The role of these defects may be mediated during the phase transition by direct coupling to the primary order parameter (spontaneous polarization), and/or by indirect coupling through the elastic strain. Because of the large tetragonal distortion of lead titanate, it seems likely that the latter interaction is the dominant one. Phenomena due to strain coupling through defects has been identified as important in a wide variety of structural phase transitions [34].

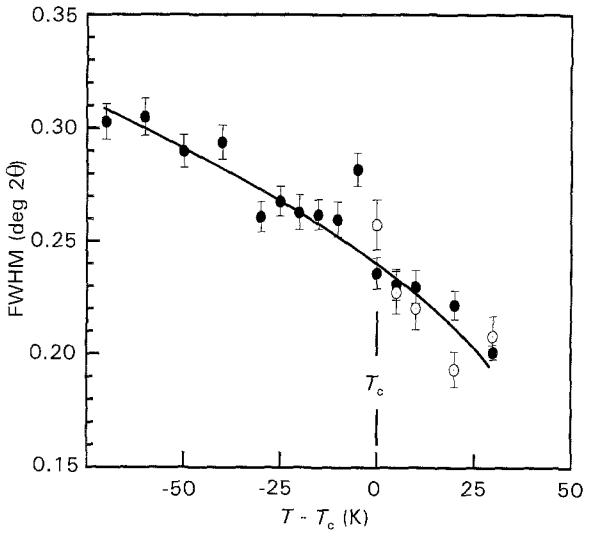


*Figure 13* Temperature dependence of the FWHM of (●) 2 2 2 and (○) 3 0 0 reflections of $Pb_{1-1.5y}La_y$ [Ti]$O_3$ ($y = 0.05$).

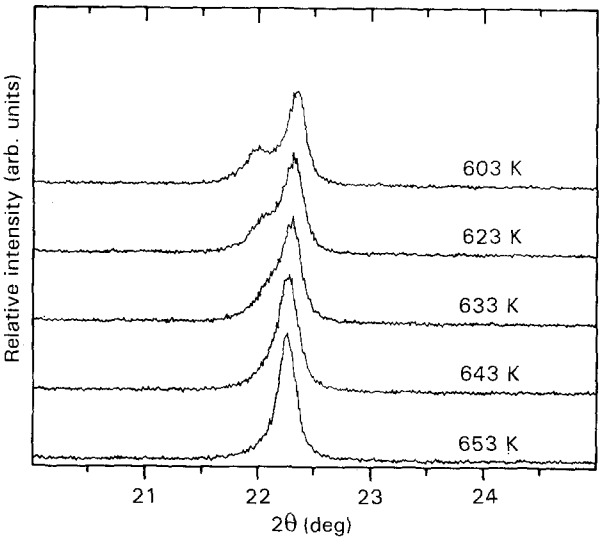


*Figure 14* Temperature dependence of 0 0 1/1 0 0 reflections of $Pb_{1-1.5y}La_y$ [Ti]$O_3$ ($y = 0.05$). (Cu $K_{\alpha_1}$ radiation).

When small amounts ($y \leqslant 0.01$) of lanthanum are first introduced into the lattice, the defects are widely separated. The degree of interaction between the defects will be primarily determined by the strength of the defect fields, by the characteristic range of interaction, and by the temperature relative to $T_c$ [35, 36]. The fact that no "plateau" effect (a range of composition over which the transition temperature does not renormalize) was observed for lanthanum concentrations as low as 0.5 at% indicates that the defects interact strongly with the lattice [35].

For these specimens, a strong asymmetry and temperature-dependent broadening was observed in the X-ray diffraction profiles. The associated changes in the elastic properties of the lattice appeared to be connected with the sharp decrease in the transition enthalpy. These observations are consistent with an analysis [37] of the Devonshire energy function [10] for lead titanate [8], which predicts a strong decrease in the first-order character of the transition resulting from even subtle changes in elastic or electrostructure behaviour. The initial loss in the first-order character of the transition observed in the calorimetry data has also been reported for lanthanum-doped single-crystal specimens [21], as well as for lead titanate specimens into which lattice defects have been deliberately introduced by processing [15, 16].

At higher dopant levels ($y \geqslant 0.02$), a clear change in the mode by which the lanthanum or vacancies were accommodated was observed. This behaviour was signalled by the abrupt increase in the symmetry of the diffraction profiles (Fig. 4) and by the onset of the departure of the lattice parameters from Vegard's law (Fig. 5). Transmission electron microscopy confirmed that the lattice relaxation mechanism involved a non-uniform distribution of the crystal tetragonality that manifested itself in a progressive complication of the ferroelectric domain structure. As the extent of the sub-domain texture increased, the character of the

transition became more diffuse. Indeed, the changes in domain texture as seen in Fig. 9 have been recently shown [38] to correlate well with the degree of deviation of the dielectric response from the expected Curie–Weiss behaviour [22]. Similar microstructures are also observed in lanthanum-substituted lead zirconate–titanate compositions having diffuse transitions [39]. The implications of these modulated domain structures with respect to the crystal symmetry and phase transition behaviour have been recently discussed in more detail.

## 5. Summary

The phase transition behaviour and structural characteristics of lanthanum-substituted lead titanate ferroelectrics were investigated by high-temperature X-ray diffraction and differential scanning calorimetry. Interconnections between the phase transition behaviour, the ferroelectric domain structure and the dielectric properties were identified. The results demonstrated the important influence of elastic strain coupling through lanthanum/vacancy-induced defect fields on the first-order character of the transition. The initial relaxation of the lattice to these fields manifested itself in a substantial decrease in the signature first-order discontinuity of the phase transition. Associated with this relaxation process was the development of a modulated ferroelectric domain structure, the appearance of which correlated well with the onset of the diffuse phase transition behaviour. It was suggested that further degeneration of the domain structure into tweed textures is responsible for the anomalous dielectric response near the phase transition.

## Acknowledgements

The authors are indebted to the Office of Naval Research for providing financial support for this research. The transition enthalpy measurements were carried out in the Calorimetry Laboratory of Professor A. Navrotsky at Princeton University and were supported by the NSF grant DMR 92-15802.

## References

1. A. M. GLAZER and S. A. MABUD, *Acta. Crystallogr.* **B34** (1978) 1065.
2. G. A. SAMARA, *Ferroelectrics* **2** (1972) 277.
3. G. BURNS and B. A. SCOTT, *Phys. Rev. Lett.* **25** (1970) 1191.
4. M. E. LINES and A. M. GLASS, "Principles and Applications of Ferroelectrics and Related Materials" (Clarendon, Oxford, 1977) p. 248.
5. R. J. NELMES, R. O. PILTZ, W. F. KUHS, Z. TUN and R. RESTORI, *Ferroelectrics* **108** (1990) 165.
6. E. G. FESENKO, V. G. GAVRILYACHENKO and E. V. ZAROCHENTSEV, *Izv. Akad. Nauk SSSR Ser. Fiz.* **34** (1970) 2541.
7. *Idem, Bull. Acad Sci. USSR* **34** (1970) 2262.
8. M. J. HAUN, E. FURMAN, S. J. JANG, H. A. McKINSTRY and L. E. CROSS, *J. Appl. Phys.* **62** (1987) 3331.
9. G. A. ROSSETTI Jr, K. R. UDAYAKUMAR, M. J. HAUN and L. E. CROSS, *J. Amer. Ceram. Soc.* **73** (1990) 3334.
10. A. F. DEVONSHIRE, *Adv. Phys.* **3** (1954) 85.
11. S. A. MABUD and A. M. GLAZER, *J. Appl. Crystallogr.* **12** (1979) 49.
12. G. SHIRANE, R. PEPINSKY and B. C. FRAZER, *Acta. Crystallogr.* **9** (1956) 131.
13. S. C. ABRAHAMS, S. K. KURTZ and P. B. JAMIESON, *Phys. Rev.* **172** (1968) 551.
14. V. G. GAVRILYACHENKO, R. I. SPINKO, M. A. MARTYNENKO and E. G. FESENKO, *Sov. Phys. –Solid State* **12** (1970) 1203.
15. S. SHIRASAKI, *Solid State Commun.* **9** (1971) 1217.
16. S. SHIRASAKI, K. TAKAHASHI and K. KAKEGAWA, *J. Amer. Ceram. Soc.* **56** (1973) 430.
17. D. HENNINGS, *Mater. Res. Bull.* **6** (1971) 329.
18. D. HENNINGS and K. H. HÄRDTL, *Phys. Status Solidi (a)* **3** (1970) 465.
19. R. J. NELMES and A. KATRUSIAK, *J. Phys. C: Solid State Phys.* **19** (1986) L725.
20. R. RAMIREZ, M. F. LAPEÑA and J. A. GONZALO, *Phys. Rev.* **B42** (1990) 2604.
21. K. WOJCIK, *Ferroelectrics* **99** (1989) 5.
22. K. KEIZER, G. J. LANSINK and A. J. BURGGRAAF, *J. Phys. Chem. Solids* **39** (1978) 59.
23. G. BURNS and B. A. SCOTT, *Solid State Commun.* **13** (1973) 417.
24. G. BURNS, *Phys. Rev.* **B13** (1976) 215.
25. R. MERLIN, J. A. SANJURJO and A. PINCZUK, *Solid State Commun.* **16** (1975) 931.
26. T. W. DEKLEVA, J. M. HAYES, L. E. CROSS and G. L. GEOFFROY, *J. Amer. Ceram. Soc.* **71** (1988) C280.
27. J. B. BLUM and S. R. GURKOVICH, *J. Mater. Sci.* **20** (1985) 4479.
28. M. M. HALL Jr, V. G. VEERARGHAVAN, H. RUBIN and P. G. WINCHELL, *J. Appl. Cryst.* **10** (1977) 66.
29. B. HEMINGWAY, *Amer. Mineralogist* **72** (1987) 273.
30. C. A. RANDALL, G. A. ROSSETTI Jr and W. CAO, *Ferroelectrics* in press.
31. E. SALJE, *Phase Transitions* **34** (1991) 25.
32. C. N. W. DARLINGTON and R. J. CERNIK, *J. Phys: Condens. Matter* **3** (1992) 4387.
33. A. P. LEVANYUK and A. S. SIGOV, "Defects and Structural Phase Transitions" (Gordon and Breach, New York, 1986) p. 172.
34. S. MARAIS, V. HEINE, C. NEX and E. SALJE, *Phys. Rev. Lett.* **66** (1991) 2480.
35. E. SALJE, U. BISMAYER, B. WRUCK and J. HENSLER, *Phase Transitions* **35** (1991) 61.
36. W. CAO and J. A. KRUMHANSL, *Phys. Rev.* **B42** (1990) 4334.
37. G. A. ROSSETTI Jr, *Ferroelectrics* **133** (1992) 103.
38. G. A. ROSSETTI Jr, W. CAO and C. A. RANDALL, *ibid.* in press.
39. C. A. RANDALL, D. J. BARBER and R. W. WHATMORE, *J. Microsc.* **145** (1987) 275.

*Received 11 April*
*and accepted 10 May 1994*